

Induced gravitational waves from the cosmic coincidence

Shyam Balaji,^{1,2} Joseph Silk,^{2,3,4} and Yi-Peng Wu¹

¹*Laboratoire de Physique Théorique et Hautes Energies (LPTHE),
UMR 7589 CNRS & Sorbonne Université, 4 Place Jussieu, F-75252, Paris, France*

²*Institut d'Astrophysique de Paris, UMR 7095 CNRS & Sorbonne Université, 98 bis boulevard
Arago, F-75014 Paris, France*

³*Department of Physics and Astronomy, The Johns Hopkins University, 3400 N. Charles Street,
Baltimore, MD 21218, U.S.A.*

⁴*Beecroft Institute for Particle Astrophysics and Cosmology, University of Oxford, Keble Road,
Oxford OX1 3RH, U.K.*

E-mail: sbalaji@lpthe.jussieu.fr, silk@iap.fr, ywu@lpthe.jussieu.fr

ABSTRACT: The induced gravitational wave (GW) background from enhanced primordial scalar perturbations is one of the most promising observational consequences of primordial black hole (PBH) formation from inflation. We investigate the induced GW spectrum Ω_{IGW} from single-field inflation in the general ultra-slow-roll (USR) framework, restricting the peak frequency band to be inside 10^{-3} -1 Hz and saturating PBH abundance to comprise all dark matter (DM) in the ultralight asteroid-mass window. By invoking successful baryogenesis driven by USR inflation, we verify the viable parameter space for the specific density ratio between baryons and PBH DM observed today, the so-called “cosmic coincidence.” We show that the cosmic coincidence requirement bounds the spectral index n_{UV} in the high frequency limit, $\Omega_{\text{IGW}}(f \gg 1) \propto f^{-2n_{\text{UV}}}$, into $0 < n_{\text{UV}} < 1$, which implies that baryogenesis triggered by USR inflation for PBHs in the mass range of 10^{-16} - $10^{-12} M_{\odot}$ can be tested by upcoming Advanced LIGO and Virgo data and next generation experiments such as LISA, Einstein Telescope, TianQin and DECIGO.

Contents

1	Introduction	1
2	Generalised ultra-slow-roll inflation	2
3	Baryogenesis triggered by the ultra-slow-roll transition	4
3.1	Time evolving scalar masses	5
3.2	Final baryon asymmetry	8
4	The cosmic coincidence of dark matter and baryons	9
4.1	Primordial black hole dark matter	9
4.2	The cosmic coincidence	12
4.3	Implications for the gravitational wave background	13
4.3.1	Induced gravitational wave production	13
4.3.2	Non-Gaussian corrections	17
4.3.3	Gravitational waves from binary mergers	18
5	Conclusion	18
A	The power spectrum of induced tensor perturbations	19

1 Introduction

The cosmological gravitational wave (GW) background induced by scalar-type density fluctuations at non-linear orders must exist in all viable scenarios for the early universe [1–19] (see [20] for a recent review). In most of the scenarios, such as inflationary models or alternatives, the induced GWs generated by primordial scalar perturbations at second order are already too small and thus very challenging to observe [4–7], yet exciting opportunities still exist for future space-based telescopes that may search for largely enhanced GW spectra that are closely related to primordial black hole (PBH) formation [8–13, 21–24].

Since the first detection of GW events from a binary-black-hole merger in 2016 [25], PBHs have turned into compelling dark matter (DM) candidates [26] and the mass windows allowed for PBHs to comprise all DM have been severely constrained by observations (see [27–29] for recent reviews). Given that the largely enhanced scalar power spectrum on small scales from inflation manifests the mainstream scenario for PBH formation, the induced GW background from these inflationary models is considered one of the most promising signatures of PBH DM, flourishing many intensive investigations [30–48]. Currently, the viable window for PBH DM in the ultralight asteroid-mass range seems to put the peak amplitude of the induced GW spectrum inside the joint frequency band (10^{-4} – 10^3 Hz) for

LIGO and the next-generation experiments [49], such as Einstein Telescope (ET) [50], LISA [51, 52] and DECIGO [53, 54].

However, if we suppose that PBHs indeed occupy a significant fraction of the DM density in today’s universe, they will exhibit a surprisingly similar amount of energy density relative to that of the baryons and thus they are inevitably confronted by the so-called “cosmic coincidence problem,” as is the case for all other DM candidates. The cosmic coincidence problem can provide a good motivation to consider PBH DM as a consequence of inflation, due to the recent theoretical validation of successful baryogenesis triggered by single-field inflationary models for PBH formation [55, 56].

In this work, we investigate baryogenesis from single-field inflation with an enhanced power spectrum for curvature perturbations on small scales driven by the ultra-slow-roll (USR) transition of the rolling dynamics of the inflaton field. We consider baryon asymmetry created by the Affleck-Dine (AD) mechanism, but we relax the constant-mass assumption for the AD field used in Refs. [55, 56] so that it is possible to adopt a more general inflationary power spectrum away from the exact USR limit. This is to say that the inflationary spectrum can have a very sharp power-law decay on small scales (from its peak amplitude), which is favourable for PBH formation with a monochromatic mass spectrum. We review the general USR spectrum in Section 2.

After solving the generalised coherent motion of the AD field during inflation, we obtain the initial conditions for computing the final baryon asymmetry in the radiation dominated epoch, as provided in Section 3. In Section 4, we explore the modified parameter space from successful baryogenesis through general USR inflation and clarify its indication to the cosmic coincidence problem (Section 4.2). We compute the spectrum of the induced GWs associated with the input USR inflation and we discuss prospects for the validity of the “cosmic coincidence” residing in the PBH DM paradigm and the implications for current and future experiments. For completeness, we address in Section 4.3.2 the corrections to the induced GW spectrum led by non-Gaussianity of the curvature perturbations and we briefly illustrate the GW counterpart that result from the binary PBHs mergers in this scenario. Finally, our conclusions are provided in Section 5.

2 Generalised ultra-slow-roll inflation

In this work, we consider PBH formation from single-field models of inflation that experience a transient USR phase with largely enhanced curvature perturbation ζ on very small scales. The pivot scale k_0 that denotes the peak position of the power spectrum $P_\zeta(k)$ should be in the range of $k_0 \sim 10^{12} - 10^{15} \text{ Mpc}^{-1}$ so that the resulting PBHs formed during radiation domination are inside the ultra-light asteroid-mass window $M_{\text{PBH}}/M_\odot \sim 10^{-16} - 10^{-12}$ and they are still allowed to account for all dark matter. The three most relevant parameters that one should keep in mind throughout this work, are defined as

$$\delta \equiv \frac{\ddot{\phi}}{H\dot{\phi}}, \quad \Delta N \equiv N_* - N_0, \quad N_{\text{end}}, \quad (2.1)$$

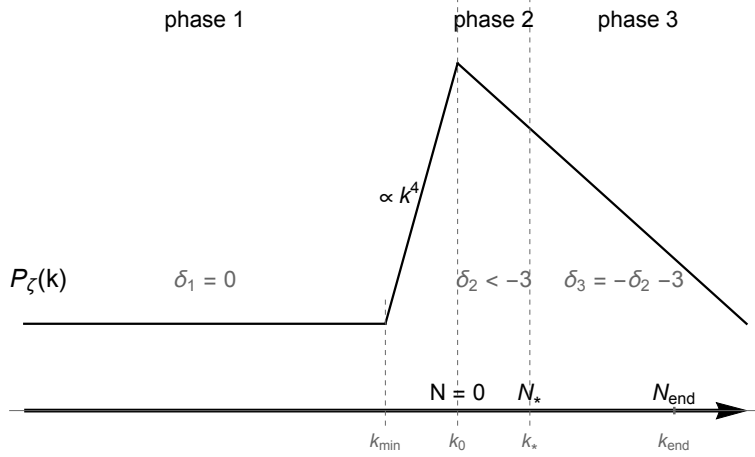


Figure 1. The broken power-law template for the power spectrum of the curvature perturbation P_ζ based on a 3-stage inflation. The rate-of-rolling $\delta_1 = 0$ is used in the primary slow-roll phase (phase 1) and $\delta_2 < -3$ in the transient ultra-slow-roll (USR) phase (phase 2) is allowed to be away from the exact ultra-slow-roll limit ($\delta_2 = -3$). The post-USR phase (phase 3) exhibits a continuous scaling from phase 2 yet it must be an acceleration phase with $\delta_3 = -\delta_2 - 3 > 0$ to terminate inflation.

where δ parametrises the rate of rolling of inflaton ϕ , ΔN measures the duration of the USR phase and N_{end} is the e-fold number at the end of inflation. For convenience, we set the e-fold number $N_0 = 0$ at which the pivot scale k_0 crosses the horizon.

As shown in Figure 1, the generic scaling behavior of the power spectrum P_ζ as a function of k can be summarized by a template of the broken power-law form [31, 57–62]

$$P_\zeta(k) = \begin{cases} A_{\text{CMB}} & k < k_{\text{min}}, \\ A_{\text{PBH}}(k/k_0)^4, & k_{\text{min}} < k < k_0, \\ A_{\text{PBH}}(k/k_0)^{6+2\delta_2}, & k > k_0, \end{cases} \quad A_{\text{PBH}} = A_{\text{CMB}} \left(\frac{k_0}{k_*} \right)^{6+4\delta_2}. \quad (2.2)$$

Where $A_{\text{CMB}} = \frac{H_*^2}{\epsilon_{\text{CMB}} M_P^2} \approx 2.2 \times 10^{-9}$ is measured by CMB experiments and k_* is the comoving scale that crosses the horizon at $N = N_*$ (the end of the transient USR phase). The duration of the USR phase is $\Delta N = \ln \frac{a_*}{a_0} = \ln \frac{k_*}{k_0}$.

The broken power-law template given by (2.2) includes three phases of inflation, which are denoted as the primary slow-roll phase (phase 1), the transient USR phase (phase 2) for enhancing the amplitude of the power spectrum and the post-USR phase (phase 3) with $\delta > 0$ that can terminate inflation. It is remarkable that the curvature perturbation ζ_k in the range of $k_{\text{min}} \leq k < k_0$ are modes that have exited the horizon in phase 1, where $k_{\text{min}} \approx k_0 \left(\frac{k_0}{k_*} \right)^{-3/2-\delta_2}$. These modes undergo superhorizon evolution after the USR transition into phase 2 [60], and eventually settle in the final boundary measured at the end of inflation as a $P_\zeta \sim k^4$ growth [58, 59, 63]. The $P_\zeta \sim k^4$ growth is a consequence of entropy perturbation domination [64], which is the criterion for breaking the initial scaling

power $P_\zeta \sim k^0$ led by phase 1 [61, 63].¹ On the other hand, the entropy domination does not occur in most of the single-field models across the transition from phase 2 to 3 so that $P_\zeta(k)$ exhibits a continuous scaling in the power of k till the end of inflation. This adiabatic condition fixes the rate-of-rolling in phase 3 as $\delta_3 = -\delta_2 - 3$ [61].

The previous studies [55, 56] considered a transient quasi-USR phase with $-3.2 \lesssim \delta_2 < -3$ to sustain the constant-mass approximation for the charged scalar that is responsible for creating the baryon asymmetry. In this work, we relax such a restriction by considering a general value allowing for $\delta_2 \ll -3$.² There can be at least two benefits for constructing the scenario in the region of $\delta_2 \ll -3$. First, the effective mass of the inflaton in phases 2 and 3 reads $\frac{m_\phi^2}{H_*^2} \approx -\delta(\delta + 3)$ [56, 61] (assuming constant δ), where m_ϕ is continuous across the two phases as protected by the scaling condition $\delta_3 = -\delta_2 - 3$. Taking $\delta_2 \ll -3$ thus gives $m_\phi/H_* \gg 1$, which is expected to significantly reduce the effect of quantum diffusion in the exact USR case with $\delta_2 = -3$ [65–67]. Second, $P_\zeta(k > k_0) \sim k^{6+2\delta_2}$ with $\delta_2 \ll -3$ decays sharply in the large k limit, leading to a narrow peak at $k = k_0$. As shown in Section 4.1, such a narrow-peak spectrum can transfer into a narrow distributed mass function for PBHs, which is more appropriate (although still not quite accurate) when comparing with most of the observational constraints in which the monochromatic PBH mass assumption is generically applied.

3 Baryogenesis triggered by the ultra–slow–roll transition

The breakdown of the constant mass approximation [56] for the charged scalar is the price to pay for entering into the $\delta_2 \ll -3$ regime. In this section, we investigate the coherent motion of the charged scalar with time-varying mass induced by the transient USR transition. Given that we consider the charged scalar, σ , as the source field for generating baryon asymmetry via the AD mechanism, we also identify σ as the AD field.

As introduced in Ref. [56], we consider σ possessing a $U(1)$ baryon number given by $n_B = j^0 = i(\sigma^* \dot{\sigma} - \sigma \dot{\sigma}^*)$. The dynamics of inflaton ϕ enters the effective mass of σ through derivative couplings described in the Lagrangian

$$\mathcal{L}_\sigma = |\partial\sigma|^2 + m_\sigma^2 |\sigma|^2 + \frac{c_1}{\Lambda} |\sigma^2| \square\phi + \frac{c_2}{\Lambda} \partial_\mu \phi [\sigma \partial^\mu \sigma + \sigma^* \partial^\mu \sigma^*] + \frac{c_3}{\Lambda^2} (\partial\phi)^2 |\sigma|^2, \quad (3.1)$$

¹The domination of entropy mode in ζ is so far a sufficient condition for violating the continuity of the momentum scaling Δ in the power spectrum as $P_\zeta \sim k^{2\Delta}$ is protected by the dilatation symmetry of the de Sitter background. Note that $\Delta = 3/2 - |3/2 + \delta| \rightarrow 0$ in the slow-roll and exact USR inflation with $\delta = 0$ or $\delta = -3$, respectively. It is interesting to seek other mechanisms that can break the scaling power Δ in single-field inflation.

²In single-field inflation, the rolling rate $\delta < -3$ is generally realized from inflaton ϕ to climb up a little bump in the potential $V(\phi)$ that exhibits a tachyonic mass ($\partial_\phi^2 V < 0$ and $\partial_\phi V > 0$) region. A transient off-attractor phase is usually required for the inflaton to obtain enough kinetic energy to climb up the bump. Such an off-attractor phase with increasing kinetic energy results in a generic dip feature in the power spectrum right before the k^4 growth. However, this dip feature in the power spectrum has little effect on the PBH abundance or the baryogenesis process considered in this work, so it can be removed by considering the broken power-law template (2.2) for simplicity. As reflected from the discussion in Section 4, our scenario in fact focuses on the regime of $-4 < \delta < -3$ where the possible kinetic energy domination (with $\epsilon_H \sim \mathcal{O}(1)$) due to the off-attractor phase is negligibly short.

where c_1, c_2, c_3 are $\mathcal{O}(1)$ coupling constants. The Lagrangian (3.1) is C/CP invariant but the c_2 term violates baryon number. Note that the imaginary phase in c_2 can be absorbed into the phase term of σ . The cutoff scale Λ should be in the range of $H_* \ll \Lambda \leq M_P$ to justify the effective field theory description during inflation.

To study the coherent motion of the AD field, it is more convenient to decompose the Lagrangian into the mass eigenstates σ_{\pm} via $\sigma \equiv \frac{\sigma_- + i\sigma_+}{\sqrt{2}}$, where (3.1) becomes a system of two real scalars as

$$\begin{aligned} \mathcal{L}_{\pm} = & \frac{1}{2} (\partial\sigma_+)^2 + \frac{1}{2} \left[m_{\sigma}^2 + \frac{c_1 + c_2}{\Lambda} \square\phi + \frac{c_3}{\Lambda^2} (\partial\phi)^2 \right] \sigma_+^2 \\ & + \frac{1}{2} (\partial\sigma_-)^2 + \frac{1}{2} \left[m_{\sigma}^2 + \frac{c_1 - c_2}{\Lambda} \square\phi + \frac{c_3}{\Lambda^2} (\partial\phi)^2 \right] \sigma_-^2. \end{aligned} \quad (3.2)$$

The effective masses are therefore controlled by the coherent motion of ϕ , where

$$m_{\pm}^2 = m_{\sigma}^2 + \frac{c_1 \pm c_2}{\Lambda} \square\phi + \frac{c_3}{\Lambda^2} (\partial\phi)^2. \quad (3.3)$$

We note that the necessary CP violation for successful baryogenesis is spontaneously realised by the emergence of a CP-violating initial VEV in a local universe [68, 69] (similar to the idea of spontaneous T violation [70]).

3.1 Time evolving scalar masses

Let us now apply the inflationary background with the transient USR transition introduced in Section 2. Based on the definitions in Eq. (2.1), we get the equations of motion

$$\square\phi = -\ddot{\phi} - 3H\dot{\phi} \approx -(\delta + 3)\sqrt{2\epsilon_H}M_P H_*^2 \quad (3.4)$$

and

$$(\partial\phi)^2 = \dot{\phi}^2 \approx 2\epsilon_H M_P^2 H_*^2, \quad (3.5)$$

where $\epsilon_H = -\frac{\dot{H}}{H^2}$ is the first slow-roll parameter. Therefore, with the transition of δ in each phase of inflation, the effective masses take different values like

$$m_{i\pm}^2 = m_{\sigma}^2 + \frac{c_1 \pm c_2}{\Lambda} [-(\delta_i + 3)]\sqrt{2\epsilon_i}M_P H_*^2 + \frac{c_3}{\Lambda^2} 2\epsilon_i M_P^2 H_*^2. \quad (3.6)$$

Note that $\frac{d\ln\epsilon_H}{dN} \approx 2\delta$ and $\epsilon_1 \equiv \epsilon_H(N < 0) = \epsilon_{\text{CMB}}$ is approximately a constant. This yields $\epsilon_2 \equiv \epsilon_{\text{CMB}}e^{2\delta_2 N}$ and $\epsilon_3 = \epsilon_* e^{2\delta_3(N-N_*)}$ where $\epsilon_* \equiv \epsilon_H(N_*) = \epsilon_{\text{CMB}}e^{2\delta_2 N_*}$.

In order to address the time evolution of ϵ_i in the effective masses (3.6), we use the dimensionless parametrisation

$$M_{i\pm}^2 \equiv \frac{m_{i\pm}^2}{H_*^2} = M_{\sigma}^2 + A_{i\pm}e^{\delta_i N} + B_i e^{2\delta_i N}, \quad (3.7)$$

where $M_{\sigma} = m_{\sigma}/H_*$. $A_{i\pm}$ and B_i are dimensionless constants, and the coherent motion of the mass eigenstates in each phase, $\sigma_{i\pm}$ are governed by the equation of motion

$$\frac{d^2\sigma_{i\pm}}{dN^2} + 3\frac{d\sigma_{i\pm}}{dN} + M_{i\pm}^2(N)\sigma_{i\pm} = 0. \quad (3.8)$$

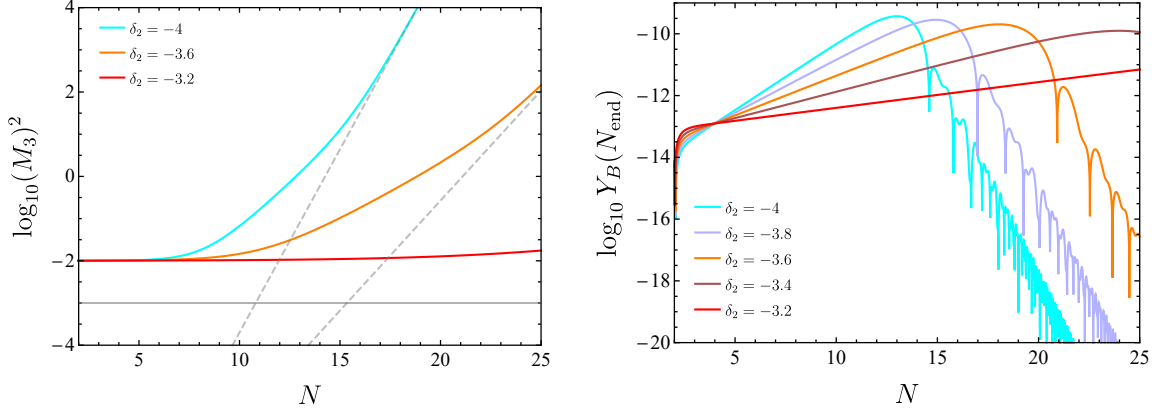


Figure 2. The time evolution of $M_3^2(N)$ (left panel) and the baryon asymmetry at the end of inflation $Y_B(N_{\text{end}})$ (right panel) with various choices of δ_2 and $\delta_3 = -\delta_2 - 3$. In both panels, $\frac{m_\sigma}{H_*} = 0.1$, $\frac{\Lambda}{M_P} = 1$, $\Delta N = N_* = 2$ are used.

The dimensionless constants are solved to be

$$A_{1,2\pm} = \frac{(c_1 \pm c_2)[-(\delta_{1,2} + 3)]\sqrt{2\epsilon_{\text{CMB}}}M_P}{\Lambda}, \quad B_1 = B_2 = \frac{2c_3\epsilon_{\text{CMB}}M_P^2}{\Lambda^2}. \quad (3.9)$$

Since $\delta_1 \rightarrow 0$ in phase 1, one can easily find that $M_{1\pm}$ are constants so that we may adopt the initial conditions from [56] as

$$\sigma_{1\pm}(N_0) = \sqrt{\frac{3}{8\pi^2} \frac{H_*^2}{m_{1\pm}}}, \quad \dot{\sigma}_{1\pm}(N_0) = 0, \quad (3.10)$$

where c_1, c_2 are chosen such that $m_{1\pm}^2$ are positive.

The general solution of (3.8) is very complicated. Fortunately, the duration of the transient USR phase (phase 2) is constrained by the PBH abundance and in fact $\Delta N = N_* < 3$ in all physical models with an arbitrary choice of statistical method. We have checked that $M_{2\pm}$ being approximately constant holds in the whole parameter space of interest for $N_* \leq 3$, and this allow us to import the constant mass results from Ref. [56], where at the of end phase 2 we have

$$\sigma_{2\pm}(N_*) = \sqrt{\frac{3}{8\pi^2} \frac{H_*^2}{m_{1\pm}} \frac{1}{2\nu_{2\pm}}} \left(\Delta_{2\pm}^+ e^{-\Delta_{2\pm}^- N_*} - \Delta_{2\pm}^- e^{-\Delta_{2\pm}^+ N_*} \right), \quad (3.11)$$

$$\left. \frac{d\sigma_{2\pm}}{dN} \right|_{N=N_*} = \sqrt{\frac{3}{8\pi^2} \frac{m_{2\pm}^2}{m_{1\pm}} \frac{1}{2\nu_{2\pm}}} \left(e^{-\Delta_{2\pm}^+ N_*} - e^{-\Delta_{2\pm}^- N_*} \right), \quad (3.12)$$

with definitions $\nu_{2\pm} = \sqrt{\frac{9}{4} - M_{2\pm}^2}$ and $\Delta_{2\pm}^\pm = \frac{3}{2} \pm \nu_{2\pm}$.

Now only the solutions for phase 3 remain. In phase 3, we restrict ourselves to the broken power-law template (2.2) with $\delta_3 = -\delta_2 - 3$, where

$$A_{3\pm} = (c_1 \pm c_2)[-(\delta_3 + 3)]\sqrt{2\epsilon_{\text{CMB}}} \frac{M_P}{\Lambda} e^{(\delta_2 - \delta_3)N_*},$$

$$B_3 = 2c_3\epsilon_{\text{CMB}} \frac{M_P^2}{\Lambda^2} e^{2(\delta_2 - \delta_3)N_*}.$$

Some examples for the time evolution of M_3^2 with respect to the e-fold number N are given in Figure 2. One can see that the B_3 term in Eq. (3.7) (illustrated by the dashed line in Figure 2) only comes to dominate the effective mass with sufficiently long duration in phase 3. Hence, if we consider the end of inflation with $N_{\text{end}} < 20$, then the B_3 term can be neglected in most cases of interest. Under this condition the solution of (3.8) reads

$$\begin{aligned} \sigma_{3\pm}(N) = & C_{31} e^{-3N/2} \Gamma\left(1 - 2\frac{\nu_\sigma}{\delta_3}\right) J_{-\frac{2\nu_\sigma}{\delta_3}}\left(\frac{2}{\delta_3} \sqrt{A_{3\pm} e^{\delta_3 N}}\right) \\ & + C_{32} e^{-3N/2} \Gamma\left(1 + 2\frac{\nu_\sigma}{\delta_3}\right) J_{\frac{2\nu_\sigma}{\delta_3}}\left(\frac{2}{\delta_3} \sqrt{A_{3\pm} e^{\delta_3 N}}\right), \end{aligned} \quad (3.13)$$

where $J_n(x)$ is Bessel function of the first kind and we have denoted $\nu_\sigma = \sqrt{\frac{9}{4} - M_\sigma^2}$. For each mass eigenstate, one can solve the coefficients C_{31} , C_{32} by matching the solutions with boundary conditions $\sigma_{2\pm} = \sigma_{3\pm}$, $\frac{d\sigma_{2\pm}}{dN} = \frac{d\sigma_{3\pm}}{dN}$ at $N = N_*$. The results are given by

$$\begin{aligned} C_{31} = & \frac{\pi}{2\delta_3} \frac{e^{3N_*/2}}{\Gamma\left(1 - \frac{2\nu_\sigma}{\delta_3}\right)} \left\{ [-2d\sigma_{2*} + (-3 + 2\nu_\sigma)\sigma_{2*}] J_{\frac{2\nu_\sigma}{\delta_3}}\left(\frac{2}{\delta_3} \sqrt{A_3 e^{\delta_3 N_*}}\right) \right. \\ & \left. - 2\sigma_{2*} \sqrt{A_3 e^{\delta_3 N_*}} J_{1+\frac{2\nu_\sigma}{\delta_3}}\left(\frac{2}{\delta_3} \sqrt{A_3 e^{\delta_3 N_*}}\right) \right\} \csc\left(\frac{2\nu_\sigma}{\delta_3} \pi\right), \end{aligned} \quad (3.14)$$

$$\begin{aligned} C_{32} = & -\frac{e^{3N_*/2}}{4\nu_\sigma \delta_3^2} \left[\frac{1}{\delta_3} \sqrt{A_3 e^{\delta_3 N_*}} \right]^{-\frac{2\nu_\sigma}{\delta_3}} \Gamma\left(-\frac{2\nu_\sigma}{\delta_3}\right) \times \\ & \left\{ 2\delta_3 \nu_\sigma [2\nu_\sigma \sigma_{2*} + (2d\sigma_{2*} + 3\sigma_{2*})] {}_0\tilde{F}_1\left[1 - \frac{2\nu_\sigma}{\delta_3}; -\frac{A_3}{\delta_3^2} e^{\delta_3 N_*}\right] \right. \\ & \left. + 4\nu_\sigma A_3 e^{\delta_3 N_*} \sigma_{2*} {}_0\tilde{F}_1\left[2 - \frac{2\nu_\sigma}{\delta_3}; -\frac{A_3}{\delta_3^2} e^{\delta_3 N_*}\right] \right\}, \end{aligned} \quad (3.15)$$

where ${}_0\tilde{F}_1[n; x] = \frac{{}_0F_1[n; x]}{\Gamma(n)}$ is the regularized confluent hypergeometric function, and $\sigma_{2*} \equiv \sigma_2(N_*)$, $d\sigma_{2*} \equiv \frac{d\sigma_2}{dN}|_{N=N_*}$ are given by (3.11) and (3.12) respectively. It is important to note that we have suppressed the notation for each mass eigenstate in C_{31} , C_{32} , A_3 , σ_{2*} and $d\sigma_{2*}$.

We can estimate the (temporal) baryon asymmetry at the end of inflation by assuming instantaneous reheating soon after $N = N_{\text{end}}$. The temperature $T_* = [\frac{30}{\pi^2 g_*} \rho_{r*}]^{1/4}$ is given by the energy density of radiation $\rho_{r*} \approx 3M_P^2 H_*^2$, where $g_* = 106.75$ is the number of relativistic degrees of freedom above 300 GeV. The baryon asymmetry is then given by

$$Y_B(N_{\text{end}}) = \frac{n_B(N_{\text{end}})}{s_*} = \frac{H_*}{s_*} \left(\sigma_{3+} \frac{d\sigma_{3-}}{dN} - \sigma_{3-} \frac{d\sigma_{3+}}{dN} \right) \Big|_{N=N_{\text{end}}}, \quad (3.16)$$

where $s_* = \frac{2\pi^2 g_* T_*^3}{45}$ is the entropy production. According to the right panel of Figure 2, one can see that in the regime of $\delta_2 \ll -3$, the A_3 term in Eq. (3.7) grows very fast in phase 3. If $M_3 \gg 1$ with sufficiently large N_{end} , the AD field starts to oscillate rapidly, which washes away the generated baryon asymmetry.

3.2 Final baryon asymmetry

Having acquired the initial conditions of the AD field at the end of inflation, in this section we compute the final baryon asymmetry in the radiation domination epoch through reheating of the universe via inflaton decay. We consider that the decay of inflaton ϕ , is dominated by a perturbative channel with the decay width Γ_I . As in the typical reheating scenario, inflation is terminated by a rapid oscillation of ϕ with an effective mass $\frac{\partial^2 V(\phi)}{\partial \phi^2} \approx m_I^2 \gg H_*^2$ so that the inflaton density $\rho_I \sim a^{-3}$ decays as dust-like matter at the beginning of reheating when $H > \Gamma_I$.

Denoting $t_{\text{end}} = 0$ as the physical time at the end of inflation, we can write down an analytic solution in the limit of $H_*(t - t_{\text{end}}) \gg 1$ as [56, 68, 71]

$$\phi(t) = \phi_{\text{max}} a^{-3/2} \cos[m_I(t - t_{\text{end}})] e^{-\Gamma_I(t - t_{\text{end}})/2}, \quad (3.17)$$

where $\phi_{\text{max}} = \frac{\Lambda_I^2}{m_I}$ is the maximal amplitude for ϕ at $t = t_{\text{end}}$ and $\Lambda_I^4 = 3M_P^2 H_*^2 = \rho_{I0}$ is the definition of the energy scale of inflation. It is easy to check that $t_r \equiv 1/\Gamma_I$ is the time scale at which the density of radiation ρ_r starts to overcome ρ_I .

Using the background evolution $\square\phi = -\ddot{\phi} - 3H\dot{\phi} \approx m_I^2\phi$ and $(\partial\phi)^2 = \dot{\phi}^2$ with $\phi(t)$ given by (3.17), we can solve the equations of motion for the mass eigenstates according to

$$\ddot{\sigma}_+ + 3H\dot{\sigma}_+ + \left(m_\sigma^2 + \frac{c_1 + c_2}{\Lambda} m_I^2 \phi + \frac{c_3}{\Lambda^2} \dot{\phi}^2\right) \sigma_+ = 0, \quad (3.18)$$

$$\ddot{\sigma}_- + 3H\dot{\sigma}_- + \left(m_\sigma^2 + \frac{c_1 - c_2}{\Lambda} m_I^2 \phi + \frac{c_3}{\Lambda^2} \dot{\phi}^2\right) \sigma_- = 0, \quad (3.19)$$

where initial conditions at the end of inflation ($N = N_{\text{end}}$) are given by (3.13). The final baryon asymmetry at some time $t_f \gg t_r$ well inside the radiation dominated epoch reads

$$Y_B(t_f) = \frac{n_B(t_f)}{s(t_f)} = \frac{45}{2\pi^2 g_* T^3(t_f)} (\sigma_+ \dot{\sigma}_- - \sigma_- \dot{\sigma}_+)_{t=t_f}. \quad (3.20)$$

Since initial conditions $\sigma_{\pm 0}$ and $\dot{\sigma}_{\pm 0}$ imported from (3.13) depend on the USR parameters δ_2 , N_* and N_{end} , the final baryon asymmetry (3.20) is therefore controlled by the inflationary scenario considered in Section 2.³

The value of N_* for successful baryogenesis $Y_B \sim 10^{-10}$ is our main concern as it is the key parameter that determines the fraction of PBH density that comprises DM (see Section 4.1). To be more precise, we are interested in finding the threshold of N_* (denoted as N_{*c}) from which the final baryon asymmetry is nearly unchanged, namely $Y_B(N_{*c}) \approx Y_B(N_* \gg N_{*c})$. Our numerical tests for various choices of δ_2 indicate that N_{*c} is not sensitive to the AD mass for $m_\sigma \lesssim H_*$ but it is significantly affected by the cutoff scale Λ . In general, the smaller the cutoff Λ , the larger the value of N_{*c} is obtained since the A_2 term in Eq. (3.7) needs a longer time to be diluted.

³Initial VEVs of the mass eigenstates can realise successful baryogenesis ($Y_B \sim 10^{-10}$) in the regime of $\sigma_{\pm 0} \ll H_*$. In contrast to the conventional scenario for AD baryogenesis from flat directions [72], initial VEVs for the AD field are usually much larger than H_* .

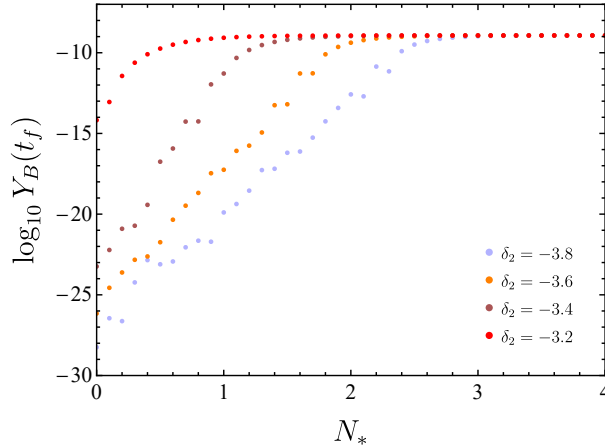


Figure 3. The final baryon asymmetry in radiation domination at $t = t_f$ with various choices of δ_2 and $\delta_3 = -\delta_2 - 3$, where $\frac{m_\sigma}{H_*} = 0.1$, $\frac{\Lambda}{M_P} = 1$ and $N_{\text{end}} = 18$ is used.

In the rest of this work, we shall focus on the highest cutoff $\Lambda = M_P$ since this gives the lowest N_{*c} possible among all the viable scenarios so that the parameter space for the constant Y_B is maximized. As shown in Figure 3, the constant Y_B plateau is recovered in the USR limit when $\delta_2 \rightarrow -3$, which are the cases investigated in Refs. [55, 56]. With the generalization of δ_2 away from -3 , the constant Y_B plateau is narrowed down towards large N_* . This result has important consequences for the “cosmic coincidence” as will be addressed in the next Section.

4 The cosmic coincidence of dark matter and baryons

CMB observations reported that the cold dark matter (CDM) density in the standard Λ CDM scenario today is $\Omega_{\text{CDM}0} = 0.265$ and the redshift at matter-radiation equality is $z_{\text{eq}} = 3402$ [73]. These findings indicate that $\Omega_{\text{CDMeq}} = 0.42$ and $\Omega_{\text{Beq}} = m_B n_{\text{Beq}} = 0.08$, where $m_B = 0.938$ GeV is the averaged nucleon mass and $n_{\text{Beq}} = |Y_B|s(t_{\text{eq}})$ is the baryon number density. The specific ratio between the two species, namely

$$\frac{\Omega_{\text{CDMeq}}}{\Omega_{\text{Beq}}} \approx 5, \quad (4.1)$$

seems to imply a non-trivial connection of their origin, since one would expect that the densities between CDM and baryons to differ by orders of magnitude if their genesis is completely uncorrelated in the early universe. Therefore the nearly $\mathcal{O}(1)$ ratio shown in Eq. (4.1) is sometimes remarked referred to as the “cosmic coincidence problem” and in this section we address a possible scenario for the cosmic coincidence in which dark matter is composed by PBHs fostered from USR inflation.

4.1 Primordial black hole dark matter

Since the inflaton decays during reheating, the enhanced curvature perturbations are inherited by the radiation density perturbations. Therefore, shortly after reentry into the

horizon in radiation domination, PBHs are formed at the high variance peaks of the density fluctuations. This is because the overdense regions will cease expanding some time after they enter the particle horizon and collapse against the pressure if they exceed the Jeans mass.

We shall focus on the viable window for PBHs to comprise all DM in the asteroid-mass range $M_{\text{PBH}} \simeq 10^{-16}\text{-}10^{-12}M_{\odot}$ which indicates that the pivot scale $k_0/k_{\text{eq}} \simeq (M_{\text{eq}}/M_{\text{PBH}})^{1/2}$ for the initiation of a USR phase in the range $k_0 \simeq 3 \times 10^{12}\text{-}10^{14} \text{ Mpc}^{-1}$, where k_{eq} and M_{eq} denote the horizon wavenumber and the horizon mass at matter–radiation equality respectively. The comoving horizon length is defined $R = 1/(aH)$ and the horizon mass is given by $M_H = \frac{4\pi\rho}{3(H)^3}$. We will define R as a function of M_H below.

Given a specific primordial scalar power spectrum $\mathcal{P}_{\zeta}(k)$, we can use standard techniques to calculate the PBH mass function $f(M)$ which characterises the fraction of PBHs constituting DM today. Here, we shall focus on scales of the density field that reenter the Hubble radius during the radiation dominated epoch. At matter–radiation equality, the PBH-to-DM density ratio is given by

$$f_{\text{PBH}} = \frac{\Omega_{\text{PBHeq}}}{\Omega_{\text{DMeq}}} = \frac{1}{\Omega_{\text{DMeq}}} \int f(M_H) d \log M_H, \quad (4.2)$$

where $f(M_H) = \frac{\beta(M_H)}{\Omega_{\text{DM}}} \left(\frac{M_{\text{eq}}}{M_H}\right)^{1/2}$ shows the PBH mass function as a function of the horizon mass at matter–radiation equality and $\beta(M_H)$ is the fraction of PBH density at the given M_H .⁴ Note that PBHs behave as dust-like matter and thus $a_{\text{eq}}/a \sim (M_{\text{eq}}/M_H)^{1/2}$ describes the relative growth of $\beta(M_H)$ during radiation domination. The scale dependent horizon mass M_H and the co–moving scale R can be written in terms of M_H as

$$M_H = M_{\text{eq}} \left(\frac{k_{\text{eq}}}{k}\right)^2 \left(\frac{g_{\text{eq}}}{g_*}\right)^{1/3}, \quad R(M_H) = \frac{1}{k_{\text{eq}}} \left(\frac{M_H}{M_{\text{eq}}}\right)^{1/2} \left(\frac{g_*}{g_{\text{eq}}}\right)^{1/6}, \quad (4.3)$$

where the horizon mass is given by $M_{\text{eq}} = 2.94 \times 10^{17}M_{\odot}$ and the number of relativistic degrees of freedom at matter–radiation equality is given by $g_{\text{eq}} = 3$, it also follows from Eq. (4.3) that $R(M_{\text{eq}}) \approx 1.57 \times 10^{40} \text{ GeV}^{-1}$. We use $k_{\text{eq}} = 0.01 \text{ Mpc}^{-1}$ and $g_* = 106.75$ since the horizon mass satisfies $M_H < 1.5 \times 10^{-7}M_{\odot}$ where the temperature of the universe exceeds 300 GeV.

If we now consider the simplest fiducial Press-Schechter statistic [76] for Gaussian fluctuations to be distributed with a dispersion σ_0 , then the rare density peaks that exceed a critical value δ_c , are responsible for production of PBHs. The fraction of energy density that collapse into BHs at the mass scale M_H during radiation domination reads

$$\beta(M_H) = 2 \int_{\nu_c} d\nu \frac{e^{-\nu^2/2}}{\sqrt{2\pi}} = \text{erfc}\left(\frac{\nu_c}{\sqrt{2}}\right) = \text{erfc}\left(\frac{\delta_c}{\sqrt{2}\sigma_0}\right), \quad (4.4)$$

⁴Strictly speaking, the PBH mass M_{PBH} can be much smaller than the horizon mass M_H at the formation epoch due to the effect of critical collapse [74, 75]. Therefore the density fraction $\beta = \beta(M_{\text{PBH}}, M_H)$ in general has a distribution in M_{PBH} at a given M_H . However, if we are only interested in the value of N_* for a fixed ratio for example, $f_{\text{PBH}} = 1$, then the difference led by critical collapse is negligible [55]. Thus, for USR inflation, we find that $M_{\text{PBH}} \approx M_H$ can be a good approximation for resolving the PBH abundance and this relation simplifies the density fraction as $\beta = \beta(M_H)$.

where $\text{erfc}(z)$ is the complimentary error function, $\nu = \delta_r/\sigma_0$ is the peak value of radiation fluctuations, and we take the critical value $\delta_c = 0.45$ from [77]. Based on the linear relation $P_{\delta_r} = (\frac{4}{9})^2 (kR)^4 P_\zeta$ in our fiducial estimation, the variance $\sigma_0^2(R)$ for a given power spectrum \mathcal{P}_ζ is computed by

$$\sigma_0^2(R) = \int_0^\infty \frac{dq}{q} \left(\frac{4}{9}\right)^2 \left[(qR)^4 P_\zeta(q) W^2(qR) T^2(qR) \right], \quad (4.5)$$

where the window function $W(qR)$ and the transfer function $T(qR)$ contained in the kernel of integral are given by

$$W(qR) = e^{-\frac{q^2 R^2}{2}}, \quad T(qR) = \frac{9\sqrt{3}}{(qR)^3} \left(\sin \frac{qR}{\sqrt{3}} - \frac{qR}{\sqrt{3}} \cos \frac{qR}{\sqrt{3}} \right), \quad (4.6)$$

respectively. Here we choose the volume-normalised Gaussian window function with smoothing radius $R = 1/(aH)$ led by the comoving horizon at conformal time η . Therefore one can refer to R or M_H as the time parameter in this calculation. Note that $T(qR) \rightarrow 1$ as $qR \rightarrow 0$ where the q mode perturbation is well outside the horizon scale.

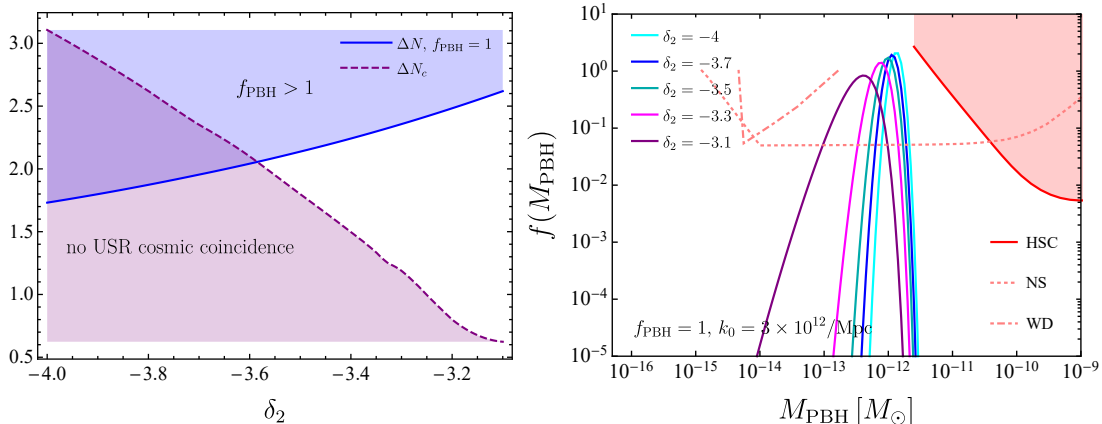


Figure 4. The ultra-slow-roll inflation duration ΔN (solid line) required for primordial black holes to saturate the total dark matter density and ΔN_c (dashed) required for the cosmic coincidence is shown as a function of the ultra-slow-roll rate δ_2 (left panel). The blue and purple shaded regions correspond to “overabundant primordial black hole dark matter” and “no clear indication to the cosmic coincidence problem from the USR triggered baryogenesis” respectively. The primordial black hole mass functions for various rates are shown (right panel), we consider a broken power-law spectrum with a pivot scale of $k_0 = 3 \times 10^{12} \text{Mpc}^{-1}$ rates of $\delta_2 = -[4, 3.7, 3.5, 3.3, 3.1]$. The constraints coming from neutron stars (NSs) and white dwarfs (WDs) are shown in dotted and dot-dashed respectively while the solid line with the upper shaded region corresponds to HSC M31 microlensing limits which are obtained from the PlotBounds [78] package.

Let us now apply the generalised USR scenario (2.2) to (4.5) to obtain the mass function $f(M)$. Note that P_ζ is only controlled by δ and ΔN and therefore $f(M)$ or f_{PBH} is not sensitive to N_{end} . In Figure 4, we show the USR duration $\Delta N = N_*$ as function of the USR rate δ_2 while ensuring that PBHs produced through USR inflation in Eq. (4.2)

saturates the DM density limit ($f_{\text{PBH}} = 1$). The explicit PBH mass functions in Figure 4 are shown for a selection of δ_2 values. We have also shown constraints for the large mass limit of the ultralight asteroid-mass window from neutron star disruption [79] and the white dwarf explosions triggering supernovae [80] as dashed and dot-dashed curves. These stellar disruption limits are not currently considered robust since having being discredited by Ref. [81]. Improving experimental limits in this mass range presents an excellent way to test the mass spectrum of PBHs produced by the cosmic coincidence. The more robust microlensing constraints for sub-planetary-mass compact objects, including PBHs, coming from Subaru HSC observations of M31 [82] are shown as the red shaded region in the right panel. This excludes PBH DM saturation above $10^{-12}M_\odot$ but loses strength at lower mass. The selection of the pivot scale k_0 , the USR rates δ_2 , and durations ΔN , largely evade the best available constraints.

4.2 The cosmic coincidence

In the regime close to the exact USR inflation scenario ($-3.2 < \delta_2 < -3$), the required duration for PBHs to account for all DM ($\Delta N > 2$, see the left panel of Figure 4) lies well within the constant Y_B plateau, as shown in Figure 3. Given that a $\mathcal{O}(0.2)$ variation in ΔN can cause around 10^{50} difference in f_{PBH} [55], the uncertainty of ΔN (for $f_{\text{PBH}} = 1$) due to various effects in the statistics of PBH abundance is at most of $\mathcal{O}(10^{-1})$ [56]. This is the reason why the coincidence ratio $\frac{\Omega_{\text{DMeq}}}{\Omega_{\text{Beq}}} \approx 5$ is rather guaranteed in this scenario despite the fact that we are using the simplest statistical method shown in Eq. (4.4).

However, with the extension of the scenario to the regime of $\delta_2 < -3.2$, the constant Y_B plateau starts to collapse towards the large ΔN limit (see Figure 3), whereas the required ΔN for $f_{\text{PBH}} = 1$ is smaller since the enhancement for A_{PBH} given in Eq. (2.2) is more efficient. As a result, one expects that the parameter space for PBH DM to drop out of the Y_B plateau with a sufficiently small δ_2 , wherein the scenario loses its indication of the cosmic coincidence as the correct baryon asymmetry also relies on tuning of other parameters.

To specify the lower bound of δ_2 for preserving the predictability of the cosmic coincidence, let us quantify the plateau threshold $\Delta N_c = N_{*c}$ by defining the edge of the constant plateau of the final baryon asymmetry as $Y_B(N_{*c}) \equiv Y_B(N_* \rightarrow \infty)/2$. For a numerical demonstration we take the asymptotic Y_B at $N_* = 4$. The results based on this definition are given in the left panel of Figure 4, where the intersection is around $\delta_2 = -3.6$. This implies that the required ΔN for $f_{\text{PBH}} = 1$ is located inside the constant Y_B plateau when $\delta_2 > -3.6$. Considering the uncertainties in the statistics of PBH abundance, we therefore impose conservative bounds for the USR rate as

$$-3.5 < \delta_2 < -3.1 \quad (\text{for the cosmic coincidence}), \quad (4.7)$$

where the conservative upper bound ensures that the effective mass of inflaton during the USR phase (phase 2) is at least of order H_* so that the effect of quantum diffusion can be largely suppressed [61].

4.3 Implications for the gravitational wave background

In this section we study the relevant GWs generated in the PBH dark matter scenario and we also investigate the implications from the cosmic coincidence to the resulting GW spectrum for current and future observations.

4.3.1 Induced gravitational wave production

Here, we are interested in calculating the GW spectral density as measured in the present universe. For a given mode in Fourier space, the frequency of GWs today is given by

$$f = \frac{k}{2\pi} = 1.55 \times 10^{-15} k \text{ Mpc Hz}. \quad (4.8)$$

With the scale crossing the Hubble radius at matter-radiation equality being $k_{\text{eq}} = 1.3 \times 10^{-2} \text{ Mpc}^{-1}$, all modes with frequencies $f \gtrsim 10^{-17} \text{ Hz}$ have re-entered the horizon during radiation domination, assuming the standard thermal history between the end of inflation and the radiation-dominated era considered in Section 3.2. For the broken power-law type spectrum adopted in Eq. (2.2), the peak frequency f_{peak} of the GW spectrum is determined by the peak scale of the curvature perturbation spectrum \mathcal{P}_ζ (namely at pivot scale k_0), which is related to the horizon mass corresponding to the pivot scale as [33]

$$f_{\text{peak}} \sim 6.7 \times 10^{-9} \left(\frac{M_H(k_0)}{M_\odot} \right)^{-1/2} \text{ Hz}. \quad (4.9)$$

Note that the central peak in the PBH mass function depends on the choice of δ_2 as one can see from the right panel of Figure 4.

The induced GWs sourced by the scalar-mode perturbation (on cosmological scales) at second order consist a stochastic background, and it is usual to describe the induced GW spectrum by energy density per logarithmic frequency interval normalized by the critical density. The dimensionless spectral density associated with the induced GWs, $\Omega_{\text{IGW}}(k, \eta)$, evaluated at late enough times when the modes are contained within the Hubble radius during the radiation dominated epoch, is given by

$$\Omega_{\text{IGW}}(k, \eta) = \frac{1}{24} \left(\frac{k}{aH} \right)^2 \overline{P_h(k, \eta)}, \quad (4.10)$$

where the conformal time is defined $\eta = (aH)^{-1}$ at horizon reentry in the radiation dominated era and the two respective polarisation modes of GWs have been summed over. P_h is the power spectrum of the induced tensor-mode perturbation sourced by linear scalar-mode perturbations at second order (A.8), which can be solved via the Green's function method [4, 5] as

$$h_\lambda(\vec{k}, \eta) = 4 \int^\eta d\eta_1 G_{\vec{k}}^-(\eta; \eta_1) \frac{a(\eta_1)}{a(\eta)} S_\lambda(\vec{k}, \eta_1), \quad (4.11)$$

where $\lambda = +, \times$ are the two polarisations, $G_{\vec{k}}^-(\eta; \eta_1) = \frac{1}{k} \sin(k(\eta - \eta_1))$ is the Green's function in radiation domination and S_λ is the source term with detailed information provided in

Appendix A. The overline in Eq. (4.10) denotes average over a few wavelengths for time oscillations led by the Green's function and the transfer function $T(k\eta)$ given in Eq. (4.6). Note that the GW density measured in today's universe, $\Omega_{\text{IGW}0}h^2$, is related to (4.10) in radiation domination like

$$\begin{aligned}\Omega_{\text{IGW}0}h^2 &= \frac{h^2}{3M_{\text{P}}^2 H_0^2} \frac{d\rho_{\text{IGW}}}{d\ln k} \\ &= \Omega_{r0}h^2 \frac{\rho_r}{\rho_{r0}} \left(\frac{a}{a_0}\right)^4 \Omega_{\text{IGW}} \\ &\approx 1.62 \times 10^{-5} \Omega_{\text{IGW}},\end{aligned}\tag{4.12}$$

where $\Omega_{r0}h^2 = 4.18 \times 10^{-5}$ is the density fraction of radiation today [73] and the factor $\frac{\rho_r(\eta)}{\rho_{r0}} \left(\frac{a(\eta)}{a_0}\right)^4 = \frac{g_*}{g_0} \left(\frac{g_*}{g_0}\right)^{-4/3} \approx 0.4$ [43, 45] is valid for $\eta \ll \eta_{\text{eq}}$ where the temperature of the universe is much higher than 300 GeV. This is correct in our case since the epoch $\eta_{k_0} = -1/k_0$ at which the pivot scale reenters the horizon for the PBH masses of interest ($k_0 = 10^{12} - 10^{14} \text{ Mpc}^{-1}$) corresponds to the temperature $T \simeq 10^6 - 10^7 \text{ GeV}$.

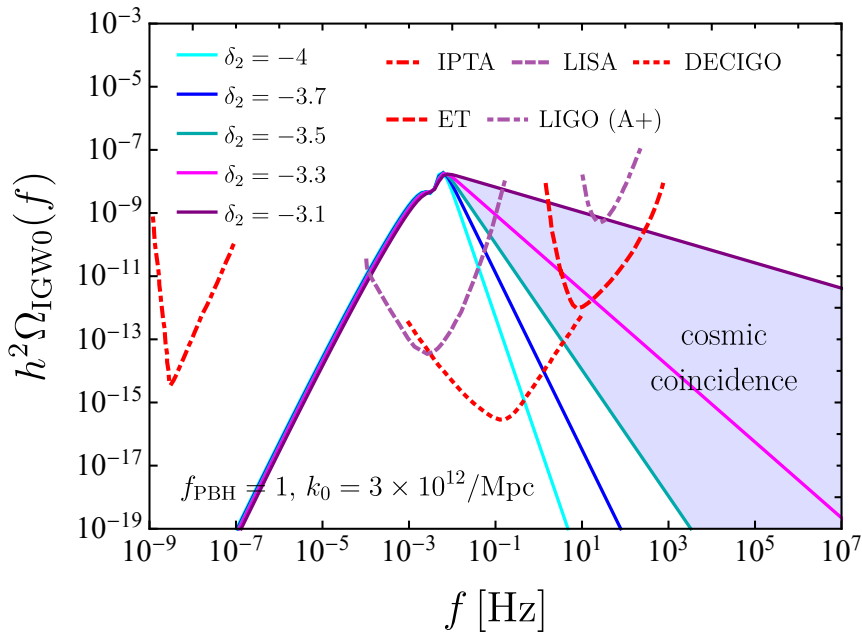


Figure 5. The present day dimensionless induced gravitational wave spectrum $h^2\Omega_{\text{IGW}0}$ is shown as a function of frequency f in Hz assuming radiation domination for ultra-slow-roll rates of $\delta_2 = -[4, 3.7, 3.5, 3.3, 3.1]$ are shown (solid lines). The shaded region between $\delta_2 = -3.1$ and $\delta_2 = -3.5$ corresponds to the cosmic coincidence region. The theoretical predictions are overlaid with relevant experimental constraints coming from IPTA (red dot-dashed), LISA (purple dashed), LIGO (A+) (purple dot-dashed), ET (red dashed) and DECIGO (red dotted). The experimental bounds are derived from the power-law integrated sensitivity curves [83] in terms of the gravitational wave spectral density for some gravitational wave detectors universe at the time of gravitational wave generation. In each case we consider a broken power-law power spectrum with pivot scale $k_0 = 3 \times 10^{12} \text{ Mpc}^{-1}$.

Using (2.2) as an input for the primordial value of the source term, we show the result of (4.10) in Figure 5 for the induced gravitational wave spectrum at present day for the same USR rate δ_2 and duration ΔN range considered in Section 4.1. We emphasise once again, that the PBHs produced during inflation ensures that the DM density of the universe is completely explained by PBHs. For the chosen pivot scale $k_0 = 3 \times 10^{12} \text{ Mpc}^{-1}$, we find the peak frequency to be around $f_{\text{peak}} \simeq 7 \times 10^{-3} \text{ Hz}$ with a peak amplitude around $\simeq 10^{-8}$.⁵ The peak in Ω_{IGW} near $k \sim 2k_0/\sqrt{3}$ is due to the resonance (of the Green's function) of the tensor perturbation with both of the scalar perturbation sources [20], where $1/\sqrt{3} = c_s$ is the sound speed of radiation and the factor two captures the second-order effect.

The induced GW spectral shape from scalar perturbations with a broken power-law spectrum has been well studied, which is indeed the case for our input in Eq. (2.2). In what follows we summarise the model-(in)dependent results with respect to the USR parameters.

The infrared (IR) tail: In the regime of $k \ll k_0$, the only contribution from our input template is $P_\zeta = A_{\text{PBH}}(k/k_0)^{n_{\text{IR}}}$ with $n_{\text{IR}} = 4$ in the range of $k_{\text{min}} < k < k_0$. This is the soft limit for the induced tensor perturbation where the main contribution is from scalar modes with $k \approx k_0$ that have been well inside the horizon. One can check that the scaling dependence in the integrand of (A.9) only comes from the transfer function $T(k\eta)$ given in Eq. (4.6), as the scalar perturbations well inside the horizon behave like plane waves. In our case, with $n_{\text{IR}} = 4$, the convolution of internal momentum of the scalar sources is dominated at the peak scale k_0 [84], where it is found that

$$\Omega_{\text{IGW}}(k \ll k_0) \sim A_{\text{PBH}}^2 \left(\frac{k}{k_0}\right)^3 \ln^2\left(\frac{k}{k_0}\right). \quad (4.13)$$

The $\Omega_{\text{IGW}} \sim \left(\frac{k}{k_0}\right)^3 \sim f^3$ behaviour manifests the stochastic nature of the signals as if the GW background is a kind of random white noise [32]. The logarithmic running $\sim \ln^2(k/k_0)$ is due to the integration over the oscillatory part of the transfer function (4.6), which is a characteristic feature of the induced GW spectrum generated during the radiation dominated universe [34]. Note that both the k^3 scaling and the logarithmic running are model independent features for the input spectrum P_ζ so that the resulting Ω_{IGW} exhibits little difference among various choices of δ_2 .

The ultraviolet (UV) tail: In the regime of $k \gg k_0$, our input template reads $P_\zeta = A_{\text{PBH}} \left(\frac{k}{k_0}\right)^{-n_{\text{UV}}}$, where the USR parameter enters the spectral index as $n_{\text{UV}} = -2\delta_2 - 6$. This regime corresponds to the generation of GWs right after horizon reentry for the scalar modes so that there is not enough time for the Green's function or the transfer function to play an important role. While the results depend on the choice of n_{UV} in general [84–86],

⁵For an input inflationary spectrum parametrised by a lognormal template with the spectral amplitude A_ζ and width Δ , we find the ratio $\frac{\Omega_{\text{IGW}}}{A_\zeta^2} < 0.01$ for the entire range of the induced GW spectrum, except for the resonance peak in the limit of $\Delta \rightarrow 0$ where the lognormal template reproduces the delta-function spectrum [35]. This is the reason why the peak amplitude of $\Omega_{\text{IGW}}^{\text{peak}} \approx A_{\text{PBH}}^2$ led by broken power-law templates considered in this work is higher than induced GW spectra provided in Refs. [20, 36, 43, 45] for PBHs as all DM.

we focus on cases with $n_{\text{UV}} < 4$ (due to the cosmic coincidence condition in Eq. (4.7) for the USR rate δ_2), in which the GW spectrum behaves as if it directly extracts the momentum dependence from the input power spectrum

$$\Omega_{\text{IGW}}(k \gg k_0) \sim A_{\text{PBH}}^2 \left(\frac{k}{k_0} \right)^{-2n_{\text{UV}}(\delta_2)}. \quad (4.14)$$

The cosmic coincidence conservative shaded parameter region between $-3.5 \leq \delta_2 \leq -3.1$ in Figure 5 corresponds to the condition (4.7) described in Section 4.2. We remark that baryogenesis triggered by USR inflation is still available even if the UV tail of the induced GW spectrum is found to be outside the shaded region. It is only that both the observed baryon asymmetry and the PBH DM rely on fine-tuning of parameters so that the scenario discussed in Section 3 has no clear resolution of the cosmic coincidence.

Observational implications: The predictions for the USR inflation model considered yields compelling GW phenomenology in the observational window of the aforementioned experiments. The relevant GW bounds include those determined by studying the time of arrival from many pulsars in space. This includes data from the pulsar timing array (PTA) [87] which is comprised of three constituent projects, the European Pulsar Timing Array (EPTA) [88], the Parkes Pulsar Timing Array (PPTA) [89], and the North American Observatory for Gravitational Waves (NANOGrav) [90], while the International Pulsar Timing Array (IPTA) [91] constraint comes from a combination of all three and covers the frequency band 10^{-9} – 10^{-7} Hz. At higher frequency, we have a band that would be observable with the advanced Laser Interferometer Gravitational Wave Observatory (aLIGO) [83] and Einstein Telescope (ET) [50], which would be sensitive to the range 10 – 10^3 Hz. In between IPTA and aLIGO/ET we expect LISA [51, 52] and DECIGO [53, 54] to be applicable. In Figure 5, we display the recently derived future sensitivity curves for ET and LISA using the latest experimental design specification computed in Ref. [92]. These are obtained by including the stochastic GW background, in contrast to model selection analyses that have discriminating power only up to the GW detector horizons. The use of the stochastic GW background to determine sensitivity curves accounts for the redshift integration of all GW signals in the universe and therefore presents a more appropriate projection for comparison with model predictions.

The current bounds on the stochastic GW background from joint LIGO and Virgo O3 data excludes $\Omega_{\text{IGW}} > 5.8 \times 10^{-9}$ in the band of 20–76.6 Hz at 2σ level [93]. Note that this is the result for the flat GW spectrum ($\alpha = 0$), from the power-law method

$$\Omega_{\text{GW}}(f) = \Omega_{\text{ref}} \left(\frac{f}{f_{\text{ref}}} \right)^\alpha, \quad (4.15)$$

where $f_{\text{ref}} = 25$ Hz and $\alpha = 2/3$ describes the stochastic background from compact binary mergers [93, 94]. The condition for the “cosmic coincidence” in Eq. (4.7) for the presented scenario translates to $-2 < \alpha < -0.2$, where the posterior strength is $\Omega_{\text{ref}} < 10^{-8}$ in this region by using the log-uniform prior. As shown in Figure 5, the UV tail of the induced GW spectrum which is realised as a consequence of PBH saturating DM (in the

ultralight asteroid mass window) from USR inflation, could be tested by the projected design sensitivity of LIGO (A+), LISA, ET, DECIGO and TianQin [95]. A measurement of the spectral index α for the stochastic GW background in the range of $-2 < \alpha < 0$ would further support the cosmic coincidence triggered by USR baryogenesis. Non-detection of the stochastic GW background by LIGO (A+) could exclude down to $\delta_2 \simeq -3.2$ for $k_0 \gtrsim 10^{14} \text{ Mpc}^{-1}$, which corresponds to a peak PBH mass smaller than $10^{-15} M_\odot$. Note that LISA, TianQin and DECIGO would be able to test the IR tail and the peak position of $\Omega_{\text{IGW}0}$ for arbitrary k_0 chosen within the PBH mass window of interest $10^{-12} - 10^{-16} M_\odot$.

4.3.2 Non-Gaussian corrections

In Section 4.3.1 above, we computed the GWs induced by a broken power-law primordial curvature power spectrum. Previously, it has been argued that the spectral tilt of the USR spectrum P_ζ in the UV regime ($k \rightarrow \infty$) is related to the magnitude of the non-Gaussianity parameter f_{NL} [96] and further argued that f_{NL} may be inferred directly from measurement of the UV tail of the induced GW spectrum [84]. Here, f_{NL} is defined according to the standard local ansatz

$$\zeta = \zeta_g + \frac{3}{5} f_{\text{NL}} \zeta_g^2, \quad (4.16)$$

where ζ_g is the Gaussian curvature perturbation considered in Section 2.

Similar to the generation of secondary tensor perturbations, the second-order curvature perturbations can be generated by non-vanishing f_{NL} which contributes to the total power spectrum as $P_\zeta = P_{\zeta_g} + P_{\zeta_g}^{\text{NG}}$, where $P_{\zeta_g}^{\text{NG}} \sim f_{\text{NL}}^2 A_{\text{PBH}}^2$. In the UV ($k \gg k_0$) and IR ($k \ll k_0$) regimes, one can follow the similar arguments as for the induced GW spectrum in Section 4.3.1 to find that

$$P_{\zeta_g}^{\text{NG}}(k \gg k_0) \sim \left(\frac{k}{k_0}\right)^{-n_{\text{UV}}}, \quad P_{\zeta_g}^{\text{NG}}(k \ll k_0) \sim \left(\frac{k}{k_0}\right)^3. \quad (4.17)$$

Note that there is no logarithmic running in the IR regime since the curvature perturbations are always computed on superhorizon scales. More detailed calculations for the non-Gaussian power spectrum of USR inflation can be found in Refs. [49, 84, 97, 98].

For the single-field inflation scenarios considered in this work, the spectral tilt can be related to the non-Gaussianity parameter by $n_{\text{UV}} = \frac{5}{12} f_{\text{NL}}$ [96] which translates to the USR parameter via

$$f_{\text{NL}} = -\frac{5}{12}(6 + 2\delta_2). \quad (4.18)$$

Even when exaggerated scenarios are considered, such as where $f_{\text{NL}} \simeq 2$ in Ref. [84], very little correction to the total curvature perturbations or to the induced GW background was realised. Our maximal value for non-Gaussianity corresponds to $f_{\text{NL}} = 5/12$ from the steepest spectral tilt of $\delta_2 = -3.5$ for the cosmic coincidence, and thus we can safely conclude that non-Gaussian corrections to Ω_{IGW} are subdominant in all cases of interest here as well.

4.3.3 Gravitational waves from binary mergers

In Section 4.3.1, we focused on the GWs induced by large primordial density fluctuations during inflation. These large fluctuations collapse to form PBHs if their RMS amplitude exceeds a threshold value. However, once PBHs have formed, they may also behave as source for other GWs independent from those produced during inflation. The other GW counterparts could be due to PBH mergers and graviton emission by Hawking evaporation [30]. We note that if PBHs are lighter than 10^{15} g they have already evaporated by today and no mergers can be resolved. PBHs heavier than 10^{15} g have not yet evaporated and their binaries could be merging in the nearby universe. We avoid detailed discussion of signals from mergers in this work due to the large astrophysical uncertainties and strong model dependence associated with such predictions. However, there do exist some basic approximations that provide very crude order of magnitude estimates of the frequency at which we expect the GWs from the mergers of PBH binaries to show up at the Innermost Stable Circular Orbit [99]

$$f_{\text{GW,max}} \approx 2f_{\text{ISCO}} \approx 4.4 \text{ kHz} \left(\frac{M_{\odot}}{M} \right), \quad (4.19)$$

where M is the total mass of the binary merger. If we consider a monochromatic PBH mass function then it follows that $M = 2M_{\text{PBH}}$. Then we may compute the approximate frequency in today's universe $f_{\text{GW,max},0} = \frac{f_{\text{GW,max}}}{1+z}$, where z denotes redshift. Hence for the PBH mergers considered in Section 4.1 of mass $\simeq 10^{-12} M_{\odot}$, we get very high frequency GWs $\gtrsim 10^{12}$ Hz that are outside the scope of even the most futuristic experimental projections.

5 Conclusion

The sharp deceleration of the slow-roll dynamics on small scales into a transient ultra-slow-roll (USR) phase is a generic mechanism to enhance the primordial power spectrum for primordial black hole (PBH) formation in single-field inflation. If PBHs indeed play an important role as dark matter (DM), the cosmic coincidence problem along with the energy densities of the universe today might hint at a correlated origin for baryons and DM. In this work, we have explored and confirmed the viability of baryogenesis, based on the Affleck-Dine (AD) mechanism, with modified initial conditions driven by a generic USR transition for PBH formation. Our results include the constant-mass AD field as a special case considered in Refs. [55, 56].

In the generalised region $\delta_2 < -3$ away from the standard USR scenario, we find asymptotically constant behavior of the final baryon asymmetry Y_B towards the large USR duration limit ($N_* \gg 1$) irrespective of the rate δ_2 . We find this to be generic feature of the model and this is directly connected to the cosmic coincidence: for PBHs to occupy a significant fraction or saturate the DM density today (or equivalently $f_{\text{PBH}} = \Omega_{\text{PBHeq}}/\Omega_{\text{CDMeq}} \lesssim 1$), the value of $N_* = \Delta N$ must be precisely fixed. The allowed parameter space of N_* for PBH DM lies well within the constant plateau region for the correct baryon asymmetry, ensuring the specific ratio $\Omega_{\text{CDMeq}}/\Omega_{\text{Beq}} \approx 5$ within statistical uncertainties of the PBH abundance [56]. However, the constant plateau for the correct baryon asymmetry narrows

with the decrease of the USR rate δ_2 from -3 , and thus PBH as all DM can be satisfied for $\Delta N \in [1.7, 2.6]$ in the corresponding range $\delta_2 \in [-3.5, -3.1]$. This is the condition for the presented scenario to provide a clear indication to the cosmic coincidence problem.

The ultralight asteroid-mass window $10^{-16} \lesssim M_{\text{PBH}}/M_{\odot} \lesssim 10^{-11}$ for PBH DM corresponds to the choice of pivot scales $k_0 \in [10^{12}, 3 \times 10^{14}] \text{Mpc}^{-1}$ for the USR template. As the most promising observational consequences of the general USR inflation, we have computed the induced gravitational wave (GW) background for $f_{\text{PBH}} = 1$ and found that it has a peak frequency $10^{-3} < f_{\text{peak}} < 1$ Hz with a maximum spectral amplitude around $h^2 \Omega_{\text{IGW0}}(f) \simeq 1 \times 10^{-8}$. The frequency scaling of the $\Omega_{\text{IGW}} \sim f^{-2n_{\text{UV}}}$ spectrum in the limit of $k \gg k_0$ (namely the UV tail) is controlled by the choice of the USR rate δ_2 (as $n_{\text{UV}} = -2\delta_2 - 6$), where the current LIGO and Virgo constraints on the stochastic GW background [93] ($\gtrsim 10^{-8}$ in the vicinity of 25 Hz) is about one order of magnitude higher than the highest UV tail for $\delta_2 = -3.1$. For PBHs comprising all DM from USR inflation in the mass window of interest, the IR tail of Ω_{IGW0} must be measured by LISA, TianQin or DECIGO. The UV tail of the induced GWs would be tested by future experiments such as LISA, Advanced LIGO and Virgo (beyond O3), the Einstein Telescope (ET) and DECIGO, regardless of whether it is compatible with the cosmic coincidence scenario considered or not.

Further more, we find that non-Gaussianity would have subdominant effects on the total curvature power spectrum and GW background since $f_{\text{NL}} = -\frac{5}{12}(6 + 2\delta_2)$ is not large enough to source noticeable corrections [84]. We also conclude that gravitational waves resulting from binary mergers would be at frequencies $f_{\text{peak}} \geq 10^{12} \text{Hz}$ which would be far too high for observation even in the most optimistic future experimental scenarios. Finally, we remark that even though the USR transition provides a striking solution to the cosmic coincidence, the fine-tuning of inflationary parameters to properly realise PBH DM inevitably remains.

Acknowledgements

We would like to thank Guillem Domènech, Jacopo Fumagalli, Gabriele Franciolini and Yoann Genolini for helpful discussions and feedback. The project has received funding from the European Union’s Horizon 2020 research and innovation programme under grant agreement No 101002846 (ERC CoG “CosmoChart”) as well as support from the Initiative Physique des Infinis (IPI), a research training program of the IDEX SUPER at Sorbonne Université.

A The power spectrum of induced tensor perturbations

We provide the complete equations for the computation of the tensor power spectrum P_h used in Eq. (4.10). Let us begin with the definition of linear perturbations in the conformal Newtonian gauge for the metric of the form

$$ds^2 = -a^2(\eta)(1 + 2\Psi)d\eta^2 + a^2(\eta) \left[(1 - 2\Phi)\delta_{ij} + \frac{1}{2}h_{ij} \right] dx^i dx^j, \quad (\text{A.1})$$

where Ψ is the Newtonian potential and Φ is the curvature potential. We define

$$h_{ij}(\vec{x}, \eta) = \int d^3k (2\pi)^{-3/2} [e_{ij}^+(\vec{k}) h_+(\vec{k}, \eta) + e_{ij}^\times(\vec{k}) h_\times(\vec{k}, \eta)] e^{i\vec{k}\cdot\vec{x}}, \quad (\text{A.2})$$

which is the linear tensor perturbation including the two polarisation modes. The transverse-traceless polarisation tensors are

$$e_{ij}^+(\vec{k}) = \frac{[e_i^1(\vec{k})e_j^1(\vec{k}) - e_i^2(\vec{k})e_j^2(\vec{k})]}{\sqrt{2}}, \quad e_{ij}^\times(\vec{k}) = \frac{[e_i^1(\vec{k})e_j^2(\vec{k}) + e_i^2(\vec{k})e_j^1(\vec{k})]}{\sqrt{2}}, \quad (\text{A.3})$$

which are expressed in terms of orthonormal basis vectors \mathbf{e}^1 and \mathbf{e}^2 orthogonal to \vec{k} .

Keeping the tensor perturbation at linear order and the linear scalar perturbations up to second order, one can obtain the equation of motion for each polarisation h_λ from the Einstein equation as

$$h_\lambda''(\vec{k}, \eta) + 2\mathcal{H}h_\lambda'(\vec{k}, \eta) + k^2 h_\lambda(\vec{k}, \eta) = 4S_\lambda(\vec{k}, \eta), \quad (\text{A.4})$$

where second-order perturbations are projected away in the transverse-traceless decomposition [5] and we have neglected the anisotropic stress in the energy momentum tensor so $\Psi = \Phi$, and thus

$$S_\lambda(\vec{k}, \eta) = \int \frac{d^3q}{(2\pi)^{3/2}} e_{ij}^\lambda(\vec{k}) q^i q^j \psi_{\vec{p}} \psi_{\vec{q}} f(p, q, \eta), \quad (\text{A.5})$$

$$f(p, q, \eta) = 2T(p\eta)T(q\eta) + \frac{4}{3(1+w)} \left[\frac{T'(p\eta)}{\mathcal{H}} + T(p\eta) \right] \left[\frac{T'(q\eta)}{\mathcal{H}} + T(q\eta) \right], \quad (\text{A.6})$$

where $\mathcal{H} = aH = \frac{2}{(1+3w)\eta}$ and w is the equation of state of the universe. $\vec{k} = \vec{p} + \vec{q}$ with $p \equiv |\vec{p}|$, $q \equiv |\vec{q}|$ are the two internal momenta. The time evolution of the scalar potential is described by $\Psi_{\vec{k}}(\eta) = T(k\eta)\psi_{\vec{k}}$ with respect to the primordial value $\psi_{\vec{k}}$, where the transfer function in the radiation dominated universe is given by (4.6). The primordial Newtonian potential $\psi_{\vec{k}}$ well outside the horizon is related to the (gauge-invariant) curvature perturbation ζ as $\psi_{\vec{k}} = \frac{3+3w}{5+3w}\zeta$, or namely

$$\langle \psi_{\vec{k}} \psi_{\vec{K}} \rangle = \delta^{(3)}(\vec{k} + \vec{K}) \frac{2\pi^2}{k^3} \left(\frac{3+3w}{5+3w} \right)^2 P_\zeta(k). \quad (\text{A.7})$$

This is where parameters of the inflationary scenario given by (2.1) enters the power spectrum of the tensor perturbation.

Solving the equation of motion (A.4) by virtue of the Green's function method (4.11), we can compute the total power spectrum of the tensor perturbation as

$$\begin{aligned} \delta^{(3)}(\vec{k} + \vec{K}) P_h(k, \eta) &= \frac{k^3}{2\pi^2} \sum_{\lambda}^{+, \times} \langle h_\lambda(\vec{k}, \eta) h_\lambda(\vec{K}, \eta) \rangle, \\ &= \frac{k^3}{2\pi^2} \int^\eta d\eta_1 G_{\vec{k}}(\eta; \eta_1) \frac{a(\eta_1)}{a(\eta)} \int^\eta d\eta_2 G_{\vec{K}}(\eta; \eta_2) \frac{a(\eta_2)}{a(\eta)} \\ &\quad \times \sum_{\lambda}^{+, \times} \langle S_\lambda(\vec{k}, \eta_1) S_\lambda(\vec{K}, \eta_2) \rangle. \end{aligned} \quad (\text{A.8})$$

Here, it is convenient to use the dimensionless variables $u \equiv p/k$, $v \equiv q/k$ and $z \equiv k\eta$ to rewrite the tensor spectrum as

$$P_h(k, z) = 4 \int_0^\infty dv \int_{|1-v|}^{1+v} du \left[\frac{v}{u} - \frac{(1-u^2+v^2)}{4uv} \right]^2 I^2(u, v, z) P_\zeta(ku) P_\zeta(kv), \quad (\text{A.9})$$

$$I(u, v, z) = \frac{9(1+w)^2}{(5+3w)^2} \int_0^z dz_1 \frac{a(z_1)}{a(z)} k G_{\vec{k}}(z, z_1) f(u, v, z), \quad (\text{A.10})$$

where our definition of $I(u, v, z)$ coincide with that defined in Ref. [30]. Note that the projection of momentum under polarisation tensors can be found in the Appendix B of Ref. [84], where

$$(e_{ij}^+ q_i q_j)^2 + (e_{ij}^\times q_i q_j)^2 = k^4 v^4 \left[1 - \frac{(1-u^2+v^2)^2}{(2v)^2} \right]^2. \quad (\text{A.11})$$

For numerical evaluation, we adopt new variables $t = u + v - 1$, $s = u - v$ introduced in Ref. [30], where $u = \frac{t+s+1}{2}$, $v = \frac{t-s+1}{2}$ and the tensor spectrum now reads

$$P_h(k, z) = 2 \int_0^\infty dt \int_{-1}^1 ds \left[\frac{t(2+t)(s^2-1)}{(1-s+t)(1+s+t)} \right]^2 \times P_\zeta\left(\frac{k(t+s+1)}{2}\right) P_\zeta\left(\frac{k(t-s+1)}{2}\right) I_{\text{RD}}^2(s, t, z). \quad (\text{A.12})$$

In the late-time limit of the radiation dominated universe i.e. where $\eta \rightarrow \infty$ and $z \gg 1$, we have the oscillation averaged result from Ref. [30] as

$$\overline{I_{\text{RD}}^2(s, t, k\eta \rightarrow \infty)} = \frac{288(-5+s^2+t(2+t))^2}{z^2(1-s+t)^6(1+s+t)^6} \times \left\{ \frac{\pi^2}{4} (-5+s^2+t(2+t))^2 \Theta\left(t - (\sqrt{3}-1)\right) + \left[-(t-s+1)(t+s+1) + \frac{1}{2}(-5+s^2+t(2+t)) \ln \left| \frac{(-2+t(2+t))}{3-s^2} \right| \right]^2 \right\}, \quad (\text{A.13})$$

where Θ is the usual Heaviside theta function. Hence the averaged analytical transfer function during radiation domination (A.13) above can be substituted into Eq. (A.12). The resulting integral will yield the oscillation averaged power spectrum $\overline{P_h(k, \eta)}$ which can be substituted into Eq. (4.10) and the dimensionless gravitational wave background to be compared with experimental limits or signals can be determined. We have verified the calculation by direct comparison with the scale invariant power spectrum normalised to unity ($A_\zeta = 1$), which yields a dimensionless gravitational wave spectrum of $\Omega_{\text{IGW}}/A_\zeta^2 = 0.822$ as expected in Ref. [30].

References

- [1] K. Tomita, *Non-Linear Theory of Gravitational Instability in the Expanding Universe*, *Progress of Theoretical Physics* **37** (05, 1967) 831–846, [<https://academic.oup.com/ptp/article-pdf/37/5/831/5234391/37-5-831.pdf>].

- [2] S. Matarrese, O. Pantano and D. Saez, *General relativistic dynamics of irrotational dust: Cosmological implications*, *Phys. Rev. Lett.* **72** (1994) 320–323, [[astro-ph/9310036](#)].
- [3] S. Matarrese, S. Mollerach and M. Bruni, *Second order perturbations of the Einstein-de Sitter universe*, *Phys. Rev. D* **58** (1998) 043504, [[astro-ph/9707278](#)].
- [4] K. N. Ananda, C. Clarkson and D. Wands, *The Cosmological gravitational wave background from primordial density perturbations*, *Phys. Rev. D* **75** (2007) 123518, [[gr-qc/0612013](#)].
- [5] D. Baumann, P. J. Steinhardt, K. Takahashi and K. Ichiki, *Gravitational Wave Spectrum Induced by Primordial Scalar Perturbations*, *Phys. Rev. D* **76** (2007) 084019, [[hep-th/0703290](#)].
- [6] P. Martineau and R. Brandenberger, *A Back-reaction Induced Lower Bound on the Tensor-to-Scalar Ratio*, *Mod. Phys. Lett. A* **23** (2008) 727–735, [[0709.2671](#)].
- [7] N. Bartolo, S. Matarrese, A. Riotto and A. Vaihkonen, *The Maximal Amount of Gravitational Waves in the Curvaton Scenario*, *Phys. Rev. D* **76** (2007) 061302, [[0705.4240](#)].
- [8] R. Saito and J. Yokoyama, *Gravitational wave background as a probe of the primordial black hole abundance*, *Phys. Rev. Lett.* **102** (2009) 161101, [[0812.4339](#)].
- [9] R. Saito and J. Yokoyama, *Gravitational-Wave Constraints on the Abundance of Primordial Black Holes*, *Progress of Theoretical Physics* **123** (05, 2010) 867–886, [<https://academic.oup.com/ptp/article-pdf/123/5/867/5435632/123-5-867.pdf>].
- [10] E. Bugaev and P. Klimai, *Induced gravitational wave background and primordial black holes*, *Phys. Rev. D* **81** (Jan, 2010) 023517.
- [11] E. V. Bugaev and P. A. Klimai, *Bound on induced gravitational wave background from primordial black holes*, *JETP Letters* **91** (Jan, 2010) 1–5.
- [12] E. Bugaev and P. Klimai, *Constraints on the induced gravitational wave background from primordial black holes*, *Phys. Rev. D* **83** (Apr, 2011) 083521.
- [13] T. Suyama and J. Yokoyama, *Temporal enhancement of super-horizon curvature perturbations from decays of two curvatons and its cosmological consequences*, *Phys. Rev. D* **84** (2011) 083511, [[1106.5983](#)].
- [14] H. Assadullahi and D. Wands, *Constraints on primordial density perturbations from induced gravitational waves*, *Phys. Rev. D* **81** (2010) 023527, [[0907.4073](#)].
- [15] H. Assadullahi and D. Wands, *Gravitational waves from an early matter era*, *Phys. Rev. D* **79** (2009) 083511, [[0901.0989](#)].
- [16] F. Arroja, H. Assadullahi, K. Koyama and D. Wands, *Cosmological matching conditions for gravitational waves at second order*, *Phys. Rev. D* **80** (2009) 123526, [[0907.3618](#)].
- [17] L. Alabidi, K. Kohri, M. Sasaki and Y. Sendouda, *Observable Spectra of Induced Gravitational Waves from Inflation*, *JCAP* **09** (2012) 017, [[1203.4663](#)].
- [18] L. Alabidi, K. Kohri, M. Sasaki and Y. Sendouda, *Observable induced gravitational waves from an early matter phase*, *JCAP* **05** (2013) 033, [[1303.4519](#)].
- [19] M. Kawasaki, N. Kitajima and S. Yokoyama, *Gravitational waves from a curvaton model with blue spectrum*, *JCAP* **08** (2013) 042, [[1305.4464](#)].
- [20] G. Domènech, *Scalar Induced Gravitational Waves Review*, *Universe* **7** (2021) 398, [[2109.01398](#)].

- [21] K. M. Belotsky, A. D. Dmitriev, E. A. Esipova, V. A. Gani, A. V. Grobov, M. Y. Khlopov et al., *Signatures of primordial black hole dark matter*, *Mod. Phys. Lett. A* **29** (2014) 1440005, [[1410.0203](#)].
- [22] T. Suyama, Y.-P. Wu and J. Yokoyama, *Primordial black holes from temporally enhanced curvature perturbation*, *Phys. Rev. D* **90** (2014) 043514, [[1406.0249](#)].
- [23] T. Nakama and T. Suyama, *Primordial black holes as a novel probe of primordial gravitational waves*, *Phys. Rev. D* **92** (2015) 121304, [[1506.05228](#)].
- [24] T. Nakama and T. Suyama, *Primordial black holes as a novel probe of primordial gravitational waves. II: Detailed analysis*, *Phys. Rev. D* **94** (2016) 043507, [[1605.04482](#)].
- [25] LIGO SCIENTIFIC COLLABORATION AND VIRGO COLLABORATION collaboration, B. P. Abbott, R. Abbott, T. D. Abbott, M. R. Abernathy, F. Acernese, K. Ackley et al., *Observation of gravitational waves from a binary black hole merger*, *Phys. Rev. Lett.* **116** (Feb, 2016) 061102.
- [26] B. Carr, F. Kuhnel and M. Sandstad, *Primordial Black Holes as Dark Matter*, *Phys. Rev. D* **94** (2016) 083504, [[1607.06077](#)].
- [27] B. Carr, K. Kohri, Y. Sendouda and J. Yokoyama, *Constraints on primordial black holes*, *Rept. Prog. Phys.* **84** (2021) 116902, [[2002.12778](#)].
- [28] B. Carr and F. Kuhnel, *Primordial Black Holes as Dark Matter: Recent Developments*, *Ann. Rev. Nucl. Part. Sci.* **70** (2020) 355–394, [[2006.02838](#)].
- [29] A. M. Green and B. J. Kavanagh, *Primordial Black Holes as a dark matter candidate*, *J. Phys. G* **48** (2021) 043001, [[2007.10722](#)].
- [30] K. Kohri and T. Terada, *Semianalytic calculation of gravitational wave spectrum nonlinearly induced from primordial curvature perturbations*, *Phys. Rev. D* **97** (2018) 123532, [[1804.08577](#)].
- [31] J. Liu, Z.-K. Guo and R.-G. Cai, *Analytical approximation of the scalar spectrum in the ultraslow-roll inflationary models*, *Phys. Rev. D* **101** (2020) 083535, [[2003.02075](#)].
- [32] R.-G. Cai, S. Pi and M. Sasaki, *Universal infrared scaling of gravitational wave background spectra*, *Phys. Rev. D* **102** (2020) 083528, [[1909.13728](#)].
- [33] R.-G. Cai, S. Pi, S.-J. Wang and X.-Y. Yang, *Pulsar Timing Array Constraints on the Induced Gravitational Waves*, *JCAP* **10** (2019) 059, [[1907.06372](#)].
- [34] C. Yuan, Z.-C. Chen and Q.-G. Huang, *Log-dependent slope of scalar induced gravitational waves in the infrared regions*, *Phys. Rev. D* **101** (2020) 043019, [[1910.09099](#)].
- [35] S. Pi and M. Sasaki, *Gravitational Waves Induced by Scalar Perturbations with a Lognormal Peak*, *JCAP* **09** (2020) 037, [[2005.12306](#)].
- [36] R.-g. Cai, S. Pi and M. Sasaki, *Gravitational Waves Induced by non-Gaussian Scalar Perturbations*, *Phys. Rev. Lett.* **122** (2019) 201101, [[1810.11000](#)].
- [37] J. Garcia-Bellido, M. Peloso and C. Unal, *Gravitational Wave signatures of inflationary models from Primordial Black Hole Dark Matter*, *JCAP* **09** (2017) 013, [[1707.02441](#)].
- [38] J. Fumagalli, S. Renaux-Petel and L. T. Witkowski, *Oscillations in the stochastic gravitational wave background from sharp features and particle production during inflation*, *JCAP* **08** (2021) 030, [[2012.02761](#)].

- [39] J. Fumagalli, S. e. Renaux-Petel and L. T. Witkowski, *Resonant features in the stochastic gravitational wave background*, *JCAP* **08** (2021) 059, [[2105.06481](#)].
- [40] C. Unal, *Imprints of Primordial Non-Gaussianity on Gravitational Wave Spectrum*, *Phys. Rev. D* **99** (2019) 041301, [[1811.09151](#)].
- [41] H. V. Ragavendra, L. Sriramkumar and J. Silk, *Could PBHs and secondary GWs have originated from squeezed initial states?*, *JCAP* **05** (2021) 010, [[2011.09938](#)].
- [42] O. Özsoy and Z. Lalak, *Primordial black holes as dark matter and gravitational waves from bumpy axion inflation*, *JCAP* **01** (2021) 040, [[2008.07549](#)].
- [43] N. Bartolo, V. De Luca, G. Franciolini, M. Peloso, D. Racco and A. Riotto, *Testing primordial black holes as dark matter with LISA*, *Phys. Rev. D* **99** (2019) 103521, [[1810.12224](#)].
- [44] Y. Tada and S. Yokoyama, *Primordial black hole tower: Dark matter, earth-mass, and LIGO black holes*, *Phys. Rev. D* **100** (2019) 023537, [[1904.10298](#)].
- [45] N. Bartolo, V. De Luca, G. Franciolini, A. Lewis, M. Peloso and A. Riotto, *Primordial Black Hole Dark Matter: LISA Serendipity*, *Phys. Rev. Lett.* **122** (2019) 211301, [[1810.12218](#)].
- [46] G. Ballesteros, J. Rey, M. Taoso and A. Urbano, *Primordial black holes as dark matter and gravitational waves from single-field polynomial inflation*, *JCAP* **07** (2020) 025, [[2001.08220](#)].
- [47] S. Wang, T. Terada and K. Kohri, *Prospective constraints on the primordial black hole abundance from the stochastic gravitational-wave backgrounds produced by coalescing events and curvature perturbations*, *Phys. Rev. D* **99** (2019) 103531, [[1903.05924](#)].
- [48] S. Kawai and J. Kim, *Primordial black holes from Gauss-Bonnet-corrected single field inflation*, *Phys. Rev. D* **104** (2021) 083545, [[2108.01340](#)].
- [49] H. V. Ragavendra, P. Saha, L. Sriramkumar and J. Silk, *Primordial black holes and secondary gravitational waves from ultraslow roll and punctuated inflation*, *Phys. Rev. D* **103** (2021) 083510, [[2008.12202](#)].
- [50] M. Maggiore et al., *Science Case for the Einstein Telescope*, *JCAP* **03** (2020) 050, [[1912.02622](#)].
- [51] P. Amaro-Seoane, *Laser interferometer space antenna*, 2017.
- [52] E. Barausse et al., *Prospects for Fundamental Physics with LISA*, *Gen. Rel. Grav.* **52** (2020) 81, [[2001.09793](#)].
- [53] K. Yagi and N. Seto, *Detector configuration of DECIGO/BBO and identification of cosmological neutron-star binaries*, *Phys. Rev. D* **83** (2011) 044011, [[1101.3940](#)].
- [54] S. Kawamura et al., *Current status of space gravitational wave antenna DECIGO and B-DECIGO*, *PTEP* **2021** (2021) 05A105, [[2006.13545](#)].
- [55] Y.-P. Wu, E. Pinetti and J. Silk, *The cosmic coincidences of primordial-black-hole dark matter*, [2109.09875](#).
- [56] Y.-P. Wu, E. Pinetti, K. Petraki and J. Silk, *Baryogenesis from ultra-slow-roll inflation*, [2109.00118](#).
- [57] G. Ballesteros, J. Rey, M. Taoso and A. Urbano, *Stochastic inflationary dynamics beyond slow-roll and consequences for primordial black hole formation*, *JCAP* **08** (2020) 043, [[2006.14597](#)].

- [58] C. T. Byrnes, P. S. Cole and S. P. Patil, *Steepest growth of the power spectrum and primordial black holes*, *JCAP* **06** (2019) 028, [[1811.11158](#)].
- [59] P. Carrilho, K. A. Malik and D. J. Mulryne, *Dissecting the growth of the power spectrum for primordial black holes*, *Phys. Rev. D* **100** (2019) 103529, [[1907.05237](#)].
- [60] S.-L. Cheng, W. Lee and K.-W. Ng, *Superhorizon curvature perturbation in ultraslow-roll inflation*, *Phys. Rev. D* **99** (2019) 063524, [[1811.10108](#)].
- [61] K.-W. Ng and Y.-P. Wu, *Constant-rate inflation: primordial black holes from conformal weight transitions*, *JHEP* **11** (2021) 076, [[2102.05620](#)].
- [62] O. Özsoy and G. Tasinato, *On the slope of the curvature power spectrum in non-attractor inflation*, *JCAP* **04** (2020) 048, [[1912.01061](#)].
- [63] S. M. Leach, M. Sasaki, D. Wands and A. R. Liddle, *Enhancement of superhorizon scale inflationary curvature perturbations*, *Phys. Rev. D* **64** (2001) 023512, [[astro-ph/0101406](#)].
- [64] S. M. Leach and A. R. Liddle, *Inflationary perturbations near horizon crossing*, *Phys. Rev. D* **63** (2001) 043508, [[astro-ph/0010082](#)].
- [65] J. M. Ezquiaga, J. García-Bellido and V. Vennin, *The exponential tail of inflationary fluctuations: consequences for primordial black holes*, *JCAP* **03** (2020) 029, [[1912.05399](#)].
- [66] D. G. Figueroa, S. Raatikainen, S. Rasanen and E. Tomberg, *Non-Gaussian Tail of the Curvature Perturbation in Stochastic Ultraslow-Roll Inflation: Implications for Primordial Black Hole Production*, *Phys. Rev. Lett.* **127** (2021) 101302, [[2012.06551](#)].
- [67] C. Pattison, V. Vennin, D. Wands and H. Assadullahi, *Ultra-slow-roll inflation with quantum diffusion*, *JCAP* **04** (2021) 080, [[2101.05741](#)].
- [68] Y.-P. Wu and K. Petraki, *Stochastic Baryogenesis*, *JCAP* **01** (2021) 022, [[2008.08549](#)].
- [69] A. Hook, *Baryogenesis in a CP invariant theory*, *JHEP* **11** (2015) 143, [[1508.05094](#)].
- [70] T. D. Lee, *A Theory of Spontaneous T Violation*, *Phys. Rev. D* **8** (1973) 1226–1239.
- [71] Y.-P. Wu, L. Yang and A. Kusenko, *Leptogenesis from spontaneous symmetry breaking during inflation*, *JHEP* **12** (2019) 088, [[1905.10537](#)].
- [72] M. Dine, L. Randall and S. D. Thomas, *Baryogenesis from flat directions of the supersymmetric standard model*, *Nucl. Phys. B* **458** (1996) 291–326, [[hep-ph/9507453](#)].
- [73] PLANCK collaboration, N. Aghanim et al., *Planck 2018 results. VI. Cosmological parameters*, *Astron. Astrophys.* **641** (2020) A6, [[1807.06209](#)].
- [74] J. C. Niemeyer and K. Jedamzik, *Near-critical gravitational collapse and the initial mass function of primordial black holes*, *Phys. Rev. Lett.* **80** (1998) 5481–5484, [[astro-ph/9709072](#)].
- [75] J. Yokoyama, *Cosmological constraints on primordial black holes produced in the near critical gravitational collapse*, *Phys. Rev. D* **58** (1998) 107502, [[gr-qc/9804041](#)].
- [76] B. J. Carr, *The Primordial black hole mass spectrum*, *Astrophys. J.* **201** (1975) 1–19.
- [77] T. Harada, C.-M. Yoo and K. Kohri, *Threshold of primordial black hole formation*, *Phys. Rev. D* **88** (2013) 084051, [[1309.4201](#)].
- [78] B. J. Kavanagh, *bradkav/pbhbounds: Release version, .*

- [79] F. Capela, M. Pshirkov and P. Tinyakov, *Constraints on primordial black holes as dark matter candidates from capture by neutron stars*, *Phys. Rev. D* **87** (2013) 123524, [[1301.4984](#)].
- [80] P. W. Graham, S. Rajendran and J. Varela, *Dark Matter Triggers of Supernovae*, *Phys. Rev. D* **92** (2015) 063007, [[1505.04444](#)].
- [81] P. Montero-Camacho, X. Fang, G. Vasquez, M. Silva and C. M. Hirata, *Revisiting constraints on asteroid-mass primordial black holes as dark matter candidates*, *JCAP* **08** (2019) 031, [[1906.05950](#)].
- [82] N. Smyth, S. Profumo, S. English, T. Jeltema, K. McKinnon and P. Guhathakurta, *Updated Constraints on Asteroid-Mass Primordial Black Holes as Dark Matter*, *Phys. Rev. D* **101** (2020) 063005, [[1910.01285](#)].
- [83] E. Thrane and J. D. Romano, *Sensitivity curves for searches for gravitational-wave backgrounds*, *Phys. Rev. D* **88** (2013) 124032, [[1310.5300](#)].
- [84] V. Atal and G. Domènech, *Probing non-Gaussianities with the high frequency tail of induced gravitational waves*, *JCAP* **06** (2021) 001, [[2103.01056](#)].
- [85] G. Domènech, *Induced gravitational waves in a general cosmological background*, *Int. J. Mod. Phys. D* **29** (2020) 2050028, [[1912.05583](#)].
- [86] G. Domènech, S. Pi and M. Sasaki, *Induced gravitational waves as a probe of thermal history of the universe*, *JCAP* **08** (2020) 017, [[2005.12314](#)].
- [87] S. Detweiler, *Pulsar timing measurements and the search for gravitational waves*, *ApJ* **234** (Dec., 1979) 1100–1104.
- [88] G. Desvignes et al., *High-precision timing of 42 millisecond pulsars with the European Pulsar Timing Array*, *Mon. Not. Roy. Astron. Soc.* **458** (2016) 3341–3380, [[1602.08511](#)].
- [89] G. Hobbs, *The Parkes Pulsar Timing Array*, *Class. Quant. Grav.* **30** (2013) 224007, [[1307.2629](#)].
- [90] M. A. McLaughlin, *The North American Nanohertz Observatory for Gravitational Waves*, *Class. Quant. Grav.* **30** (2013) 224008, [[1310.0758](#)].
- [91] J. P. W. Verbiest, L. Lentati, G. Hobbs, R. van Haasteren, P. B. Demorest, G. H. Janssen et al., *The international pulsar timing array: First data release*, *Monthly Notices of the Royal Astronomical Society* **458** (Feb, 2016) 1267–1288.
- [92] S. S. Bavera, G. Franciolini, G. Cusin, A. Riotto, M. Zevin and T. Fragos, *Stochastic gravitational-wave background as a tool to investigate multi-channel astrophysical and primordial black-hole mergers*, [2109.05836](#).
- [93] KAGRA, VIRGO, LIGO SCIENTIFIC collaboration, R. Abbott et al., *Upper limits on the isotropic gravitational-wave background from Advanced LIGO and Advanced Virgo’s third observing run*, *Phys. Rev. D* **104** (2021) 022004, [[2101.12130](#)].
- [94] LIGO SCIENTIFIC, VIRGO collaboration, B. P. Abbott et al., *Search for the isotropic stochastic background using data from Advanced LIGO’s second observing run*, *Phys. Rev. D* **100** (2019) 061101, [[1903.02886](#)].
- [95] Z.-C. Liang, Y.-M. Hu, Y. Jiang, J. Cheng, J.-d. Zhang and J. Mei, *Science with the TianQin Observatory: Preliminary results on stochastic gravitational-wave background*, *Phys. Rev. D* **105** (2022) 022001, [[2107.08643](#)].

- [96] V. Atal and C. Germani, *The role of non-gaussianities in Primordial Black Hole formation*, *Phys. Dark Univ.* **24** (2019) 100275, [[1811.07857](#)].
- [97] P. Adshead, K. D. Lozanov and Z. J. Weiner, *Non-Gaussianity and the induced gravitational wave background*, *JCAP* **10** (2021) 080, [[2105.01659](#)].
- [98] H. V. Ragavendra, *Accounting for scalar non-Gaussianity in secondary gravitational waves*, [2108.04193](#).
- [99] M. Maggiore, *Gravitational Waves. Vol. 1: Theory and Experiments*. Oxford Master Series in Physics. Oxford University Press, 2007.